Quantification of airway thickness changes in smoke-inhalation injury using *in-vivo* 3-D endoscopic frequency-domain optical coherence tomography

Sang-Won Lee,[1,5] Andrew E. Heidary,[2] David Yoon,[1] David Mukai,[1] Tirunelveli Ramalingam,[2] Sari Mahon,[1] Jiechen Yin,[3] Joseph Jing,[3] Gangjun Liu,[1] Zhongping Chen,[1,3,6] and Matthew Brenner[1,4,7]

[1]*Beckman Laser Institute, University of California, Irvine,1002 Health Sciences Rd. East, Irvine, CA 92612, USA*
[2]*OCT Medical Imaging Inc., 1002 Health Sciences Rd. East, Irvine, CA 92612, USA*
[3]*Department of Biomedical Engineering, University of California, Irvine, Irvine, CA 92697, USA*
[4]*Pumonary and Critical care Division, UC Irvine Medical Center, Orange, CA 92868, USA*
[5]*Current address: Electronics and Telecommunications Research Institute, 138 Gajeongno, Yuseong-gu, Daejeon, 305-700, Korea*
[6]*z2chen@uci.edu*
[7]*mbrenner@uci.edu*

Abstract: Smoke inhalation injury is frequently accompanied by cyanide poisoning that may result in substantial morbidity and mortality, and methods are needed to quantitatively determine extent of airway injury. We utilized a 3-D endoscopic frequency-domain optical coherence tomography (FD-OCT) constructed with a swept-source laser to investigate morphological airway changes following smoke and cyanide exposure in rabbits. The thickness of the mucosal area between the epithelium and cartilage in the airway was measured and quantified. 3-D endoscopic FD-OCT was able to detect significant increases in the thickness of the tracheal walls of the rabbit beginning almost immediately after smoke inhalation injuries which were similar to those with combined smoke and cyanide poisoning.

OCIS codes: (170.4500) Optical coherence tomography; (170.4580) Optical diagnostics for medicine; (110.4500) Optical coherence tomography; (120.5820) Scattering measurements.

References and links

1. R. A. Cox, A. S. Burke, K. Soejima, K. Murakami, J. Katahira, L. D. Traber, D. N. Herndon, F. C. Schmalstieg, D. L. Traber, and H. K. Hawkins, "Airway obstruction in sheep with burn and smoke inhalation injuries," Am. J. Respir. Cell Mol. Biol. **29**(3), 295–302 (2003).
2. D. L. Traber, H. A. Linares, D. N. Herndon, and T. Prien, "The pathophysiology of inhalation injury--a review," Burns **14**(5), 357–364 (1988).
3. D. R. Thorning, M. L. Howard, L. D. Hudson, and R. L. Schumacher, "Pulmonary responses to smoke inhalation: morphologic changes in rabbits exposed to pine wood smoke," Hum. Pathol. **13**(4), 355–364 (1982).
4. M. Eckstein, and P. M. Maniscalco, "Focus on smoke inhalation--the most common cause of acute cyanide poisoning," Prehosp. Disaster Med. **21**(2), s49–s55 (2006).
5. P. M. Maniscalco, "From Smoke Inhalation to Chemical Attacks: Acute Cyanide Poisoning in the Prehospital Setting," Prehosp. Disaster Med. **21**, s38–s39 (2006).
6. F. J. Baud, P. Barriot, V. Toffis, B. Riou, E. Vicaut, Y. Lecarpentier, R. Bourdon, A. Astier, and C. Bismuth, "Elevated blood cyanide concentrations in victims of smoke inhalation," N. Engl. J. Med. **325**(25), 1761–1766 (1991).
7. D. J. O'Brien, J. Augustine, and D. W. Walsh, "Cyanide exposure, smoke inhalation, and pre-hospital treatment: Recognizing the signs and symptoms and available treatment options," (Cyanide Poisoning Treatment Coalition, 2009). *http://www.firesmoke.org/index.php?option=com_content&view=article&id=166&Itemid=142*.
8. F. Hinder, J. Meyer, M. Booke, J. S. Ehardt, J. R. Salsbury, L. D. Traber, and D. L. Traber, "Endogenous nitric oxide and the pulmonary microvasculature in healthy sheep and during systemic inflammation," Am. J. Respir. Crit. Care Med. **157**(5 Pt 1), 1542–1549 (1998).

#136728 - $15.00 USD Received 18 Oct 2010; revised 21 Dec 2010; accepted 30 Dec 2010; published 5 Jan 2011

9. H. Zhu, B. Ka, and F. Murad, "Nitric oxide accelerates the recovery from burn wounds," World J. Surg. **31**(4), 624–631 (2007).
10. H. Ogura, D. Saitoh, A. A. Johnson, A. D. J. Mason, B. A. J. Pruitt, and W. G. J. Cioffi, ""The effect of inhaled nitric oxide on pulmonary ventilation-perfusion matching following smoke inhalation injury," J. Trauma-Injury Infect," Crit. Care **37**, 893–898 (1994).
11. R. L. Sheridan, "Airway management and respiratory care of the burn patient," Int. Anesthesiol. Clin. **38**(3), 129–145 (2000).
12. T. Muehlberger, D. Kunar, A. Munster, and M. Couch, "Efficacy of fiberoptic laryngoscopy in the diagnosis of inhalation injuries," Arch. Otolaryngol. Head Neck Surg. **124**(9), 1003–1007 (1998).
13. M. J. Masanès, C. Legendre, N. Lioret, R. Saizy, and B. Lebeau, "Using bronchoscopy and biopsy to diagnose early inhalation injury. Macroscopic and histologic findings," Chest **107**(5), 1365–1369 (1995).
14. M. J. Masanes, C. Legendre, N. Lioret, D. Maillard, R. Saizy, and B. Lebeau, ""Fiberoptic Bronchoscopy for the Early Diagnosis of Subglottal Inhalation Injury - Comparative Value in the Assessment of Prognosis," J. Trauma-Injury Infect," Crit. Care **36**, 59–67 (1994).
15. D. Huang, E. A. Swanson, C. P. Lin, J. S. Schuman, W. G. Stinson, W. Chang, M. R. Hee, T. Flotte, K. Gregory, C. A. Puliafito, and J. G. Fujimoto, "Optical coherence tomography," Science **254**(5035), 1178–1181 (1991).
16. D. C. Adler, Y. Chen, R. Huber, J. Schmitt, J. Connolly, and J. G. Fujimoto, "Three-dimensional endomicroscopy using optical coherence tomography," Nat. Photonics **1**(12), 709–716 (2007).
17. S. H. Yun, G. J. Tearney, J. F. de Boer, N. Iftimia, and B. E. Bouma, "High-speed optical frequency-domain imaging," Opt. Express **11**(22), 2953–2963 (2003), http://www.opticsinfobase.org/oe/abstract.cfm?URI=oe-11-22-2953.
18. M. A. Choma, M. V. Sarunic, C. H. Yang, and J. A. Izatt, "Sensitivity advantage of swept source and Fourier domain optical coherence tomography," Opt. Express **11**(18), 2183–2189 (2003), http://www.opticsinfobase.org/oe/abstract.cfm?URI=oe-11-18-2183.
19. G. J. Tearney, S. A. Boppart, B. E. Bouma, M. E. Brezinski, N. J. Weissman, J. F. Southern, and J. G. Fujimoto, "Scanning single-mode fiber optic catheter-endoscope for optical coherence tomography," Opt. Lett. **21**(7), 543–545 (1996), http://www.opticsinfobase.org/ol/abstract.cfm?URI=ol-21-7-543.
20. Y. T. Pan, H. K. Xie, and G. K. Fedder, "Endoscopic optical coherence tomography based on a microelectromechanical mirror," Opt. Lett. **26**(24), 1966–1968 (2001), http://www.opticsinfobase.org/ol/abstract.cfm?URI=ol-26-24-1966.
21. P. H. Tran, D. S. Mukai, M. Brenner, and Z. Chen, "In vivo endoscopic optical coherence tomography by use of a rotational microelectromechanical system probe," Opt. Lett. **29**(11), 1236–1238 (2004), http://www.opticsinfobase.org/ol/abstract.cfm?URI=ol-29-11-1236.
22. X. M. Liu, M. J. Cobb, Y. C. Chen, M. B. Kimmey, and X. D. Li, "Rapid-scanning forward-imaging miniature endoscope for real-time optical coherence tomography," Opt. Lett. **29**(15), 1763–1765 (2004), http://www.opticsinfobase.org/ol/abstract.cfm?URI=ol-29-15-1763.
23. M. Brenner, K. Kreuter, D. Mukai, T. Burney, S. G. Guo, J. P. Su, S. Mahon, A. Tran, L. Tseng, J. Ju, and Z. Chen, "Detection of acute smoke-induced airway injury in a New Zealand white rabbit model using optical coherence tomography," J. Biomed. Opt. **12**(5), 051701 (2007).
24. M. Brenner, K. Kreuter, J. Ju, S. Mahon, L. Tseng, D. Mukai, T. Burney, S. Guo, J. Su, A. Tran, A. Batchinsky, L. C. Cancio, N. Narula, and Z. Chen, "In vivo optical coherence tomography detection of differences in regional large airway smoke inhalation induced injury in a rabbit model," J. Biomed. Opt. **13**(3), 034001 (2008).
25. J. Yin, G. Liu, J. Zhang, L. Yu, S. Mahon, D. Mukai, M. Brenner, and Z. Chen, "In vivo early detection of smoke-induced airway injury using three-dimensional swept-source optical coherence tomography," J. Biomed. Opt. **14**(6), 060503 (2009).
26. J. Lee, J. Armstrong, K. Kreuter, B. J. Tromberg, and M. Brenner, "Non-invasive in vivo diffuse optical spectroscopy monitoring of cyanide poisoning in a rabbit model," Physiol. Meas. **28**(9), 1057–1066 (2007).
27. J. Su, J. Zhang, L. Yu, H. G Colt, M. Brenner, and Z. Chen, "Real-time swept source optical coherence tomography imaging of the human airway using a microelectromechanical system endoscope and digital signal processor," J. Biomed. Opt. **13**(3), 030506 (2008).
28. B. Cense, N. A. Nassif, T. Chen, M. Pierce, S. H. Yun, B. H. Park, B. E. Bouma, G. J. Tearney, and J. F. de Boer, "Ultrahigh-resolution high-speed retinal imaging using spectral-domain optical coherence tomography," Opt. Express **12**(11), 2435–2447 (2004), http://www.opticsinfobase.org/oe/abstract.cfm?URI=oe-12-11-2435.
29. U. Mahmood, N. M. Hanna, S. Han, W. G. Jung, Z. Chen, B. Jordan, A. Yershov, R. Walton, and M. Brenner, "Evaluation of rabbit tracheal inflammation using optical coherence tomography," Chest **130**(3), 863–868 (2006).
30. H. M. Loick, L. D. Traber, J. C. Stothert, D. N. Herndon, and D. L. Traber, "Smoke inhalation causes a delayed increase in airway blood flow to primarily uninjured lung areas," Intensive Care Med. **21**(4), 326–333 (1995).

1. Introduction

Airway injury due to smoke exposure and inhalation risks including thermal, chemical, and toxic injuries, as well as secondary infectious complications result in significant morbidity and mortality. In addition, critical pathophysiological alterations of airway following inhalation

#136728 - $15.00 USD Received 18 Oct 2010; revised 21 Dec 2010; accepted 30 Dec 2010; published 5 Jan 2011

burn injury patients include airway hyperemia, edema, sloughing and necrosis [1,2]. Since respiratory related symptoms and airway injury may appear as late as 2−5 days after smoke exposure, it is difficult to determine which patients will deteriorate and to monitor smoke inhalation injury patients continuously [3].

Chemical and toxic injuries caused by fire are frequently accompanied by cyanide exposure [4,5] and the extent of cyanide exposure correlates with mortality risk [6]. Hydrogen cyanide is generated under the conditions of high temperature and low oxygen in closed-space structure fires [7]. Cyanide has many effects, including inhibition of cytochrome C oxidase and inhibition of cellular oxidative metabolism affecting vital human organs such as heart and brain [4,5,7]. Treatment aimed at reversing cyanide toxicity has been advocated in smoke inhalation victims. However, combined smoke inhalation injury (with carbon monoxide exposure) and cyanide toxicity limit some potential therapeutic options, such as methemoglobin induction. The effects of the approved cyanide treatment agent, cobalamin, and the recently described novel treatment agent cobinamide, which binds nitric oxide (NO) on concurrent airway injury process in smoke inhalation injury, are not known. Because NO has been reported to have a complex role in smoke inhalation airway injury process [8–10], these NO scavengers could potentially affect airway injury when administered to patients with combined smoke and cyanide exposure and these important questions need to be investigated.

Currently, there are no highly reliable and effective diagnostic techniques to precisely assess the degree of airway injury following smoke inhalation exposure. Therefore, physicians rely on bronchoscopy and subjective clinical findings to make critical decisions regarding extent of injury, need for prophylactic intubation and ventilator support in the early period following burn and smoke exposure [11–14]. Development of a relatively non-invasive method for detecting and monitoring changes in airway injury is needed in this critical setting.

Optical coherence tomography (OCT) is a non-invasive imaging technique that provides *in-vivo* cross-sectional images of biological tissues with a high-resolution and in real-time [15,16]. OCT may provide the capability for aspects of quantitative airway injury assessment. Recently, frequency-domain OCT (FD-OCT) based on a wavelength-swept laser source has been actively used for medical applications because FD-OCT can achieve a higher acquisition speed and sensitivity than prior time-domain OCT (TD-OCT) technologies [17,18]. High-acquisition speed is needed for real-time imaging and 3-D volume rendering to minimize motion artifacts and to enable imaging of larger areas. In addition, since the penetration depth of OCT images is generally 2−3 mm, concurrent optical endoscopic probe designs based on fiber optics, and miniaturized optical and mechanical components are needed for imaging internal organs such as the trachea [19–22].

Previous OCT airway injury studies have demonstrated the capability for distinguishing changes in airway mucosal thickness following smoke exposure generated by burning of unbleached cotton [23,24]. However, since only a "single longitudinal slice" 2-D image was obtained at a specific plane using a linear movement probe, there was limited ability to control the imaging position and location precisely [23,24]. Therefore, we recently demonstrated the feasibility of using a 3-D endoscopic FD-OCT system to obtain 3-D volumetric data set acquisition, providing the ability to reconstruct volumetric data in any direction and enabling the potential for more precise detection of morphological changes in airway [25]. In this current study, we investigated the ability of 3-D endoscopic FD-OCT to obtain real-time and *in-vivo* images for quantification of thickness changes in lower tracheal airway followed by cyanide poisoning and smoke inhalation injury in control animals compared to animals with smoke injury, and combined smoke cyanide injury. The demonstration of the ability to quantitatively assess this aspect of airway injury would suggest that 3-D OCT may provide a much needed tool for determination of the effects of therapeutic interventions such as treatment of cyanide toxicity on airway injury in experimental settings and in patients.

#136728 - $15.00 USD Received 18 Oct 2010; revised 21 Dec 2010; accepted 30 Dec 2010; published 5 Jan 2011

2. Materials and methods

This protocol was approved by the UCI ARC (#2002-2397) and complied with all Federal and State regulations for animal welfare assurance. General model and preparation methods have been described previously [23,26] and are briefly summarized here.

2.1 General preparation

16 male New Zealand White rabbits with a weight of 3-5 kg (Western Oregon Rabbit Company, Philomath, OR) were studied. Each rabbit was anesthetized by intramuscular injection (IM). Ketamine HCl (100mg/ml) (Ketaject, Phoenix Pharmaceutical Inc., St. Joseph, MI) and Xylazine (20mg/ml) (Anased, Lloyd Laboratories, Shenandoa, IA), 0.75 cc/kg with a 2:1 ratio respectively, were administered intramuscularly as an anesthetic. After the IM injection, a 23 gauge 1 inch catheter was placed in the marginal ear vein to administer intravenous (IV) maintenance anesthetic of a 1:1:3 mixtures of Ketamine, Xylazine, and saline (Ketamine 100 mg/ml, Xylazine 20 mg/ml) with a rate of 0.17 ml/min as a continuous infusion.

Blunt dissection was performed to isolate the femoral artery and vein on the left thigh for blood sampling, cyanide infusion, and systemic pressure monitoring. Sodium cyanide (10 mg) was dissolved in 60 ml of 0.9% saline. Sodium cyanide solution was administered via intravenously at the rate of 1 ml/min over 60 min [26].

A dose of analgesic, Torbutrol 0.1–0.5 mg/kg SQ, was administered prior to intubation. The animals were orally intubated with a cuffed endotracheal tube of 3.5 mm out diameter and 16 cm length. In addition, we used a respirator (dual phase control respirator, model 613, Harvard Apparatus, Chicago, IL) to ventilate mechanically with FiO_2 of 100%, respiratory rate of 32 cycles/min and a tidal volume of 60 cc. A humidifier (Hudson RCI, Temecula, CA) was positioned between the ventilator and endotracheal tube to prevent drying out of the mucosa, which could result in airway changes due to prolonged exposure to ventilated O_2.

Upon completion of the experiment, the animals were euthanized with an intravenous injection of 1.0cc of Eutha-6 (390mg pentobarbital/ml) administered through the marginal ear vein.

2.2 System arterial blood pressure, blood gas analysis, and Co-oximetry

To collect blood samples and record blood pressure, femoral arterial and venous cutdowns were performed. An 18 gauge catheter (C-PMA-400-FA, Cook Inc, Bloomington, IN) was inserted into the vein and artery. A 3 way stop-cock was placed on the end of a catheter. To measure systemic arterial pressure, a calibrated pressure transducer (TSD104A Transducer and MP100 WSW System, Biopac Systems, Inc., Santa Barbara, CA) was connected to a extension tube set (Hospira, Lake Forest, IL), which was then attached to the end of the stop-cock. Blood was drawn from from both the arterial and venous catheters, and blood gas analysis performed using an IRMA SL Series 2000 Blood Analysis System (Diametrics Medical Inc., St. Paul, MN). On-site co-oximetry measurements (AVOXimeter 4000, AVOX Systems, San Antonio, TX) were conducted to measure oxy-hemoglobin, carboxy-hemoglobin, met-hemoglobin fractions and total hemoglobin. The carboxy-hemoglobin levels were analyzed to assess the degree of smoke exposure.

2.3 Administration of smoke

Smoke was administered according to the previously published protocol [23]. Unbleached cotton (70 g) was burned in a modified bee-smoker (Brushy Mountain Bee Farm, Moravian Falls, NC) for approximately 20 min. The bee-smoker was then connected to the inlet port of the mechanical ventilator with the tidal volume and ventilation rate set at 700 ml/min and 25 breaths/min, respectively. A Mylar Douglas bag (Hans Rudolph, Kansas City, MO) was connected to a second “smoke exposure” ventilator (Ventilator #2) (also a dual phase control

#136728 - $15.00 USD Received 18 Oct 2010; revised 21 Dec 2010; accepted 30 Dec 2010; published 5 Jan 2011

respirator, model 613, Harvard Apparatus, Chicago, IL) via the multiport valve to the output port in order to actively fill the bag with smoke over 25 L from the bee-smoker. The Douglas bag was then connected to the inlet port of the smoke exposure ventilator and set to a tidal volume of 60 ml/min and a ventilation rate of 18 breaths/min to deliver the (now cool) smoke from the Douglas bag to the rabbit in a controlled manner. The rabbit was disconnected from the regular ventilator (#1), and then connected to the smoke ventilator (#2) for exposure.

Smoke exposure into a rabbit was initiated after 10 min of infusion with cyanide or saline. One cycle of smoke exposure consisted of 18 breaths of cooled smoke after 9 breaths of 100% oxygen (accomplished by switching between the traditional ventilator setup and the smoke ventilator). For smoke exposure, rabbits were ventilated with 0 cycles of smoke breaths (controls) or a variable number of cycles of smoke breaths (smoke group). The smoke breaths administered was a minimum of 4 cycles and continued until carboxy hemoglobulin level has reached 30% in the blood. Co-oximetry measurements were taken at the end of every 2 smoke exposure cycles.

2.4 3-D endoscopic Fourier-domain optical coherence tomography

We used previously reported 3-D endoscopic FD-OCT system for smoke inhalation studies [25,27]. We used a swept laser (Santec Corporation, Aichi, Japan) at 1310 nm with a full-width-half-maximum of 100 nm and an output power of 5 mW. Light from the swept laser, coupled with a 1 × 2 optical coupler, was split into the sample (80%) and reference (20%) arms. Light reflected from the sample and reference arms was directed into a 2 × 2 optical coupler (50:50 split ratio) by two circulators to recombine and to use a balanced detection method. The sensitivity of this system was measured to be 107 dB. The axial scan range was 2.9 mm with a 6-dB roll-off at the depth of 2.2 mm. The axial and lateral resolutions in air were 8 μm and 20 μm, respectively. To compensate dispersion caused by the optical components, we applied a previously reported dispersion compensation algorithm based on software [28].

To obtain 3-D volumetric images of the airway, a rotational motor (Namiki Precision Jewel Co.,Ltd., Tokyo, Japan) based on a microelecromechanical system (MEMS) and a translational motorized stage (Newport Corporation, Irvine, CA) were used [25,27]. An endoscopic probe was constructed with a rotational motor, a single-mode optical fiber, a gradient index (GRIN) lens (NSG America Inc., Somerset, NJ), and 45° prism mirror (Tower Optical Corporation, Boynton Beach, FL). Light from an optical fiber was focused by the GRIN lens to a diameter of 1.3 mm and reflected to tissue by the prism mirror, which was attached on the MEMS rotational motor. The MEMS rotational motor has a diameter of 1.5 mm and a length of 9.4 mm. The probe was placed in fluorinated ethylene propylene (FEP) tubing (Zeus Inc., Orangeburg, SC) with 14 gauge and thin wall. Therefore, the outer diameter of the whole packaged probe is approximately 2.2 mm.

The sweeping speed of our swept laser is 20 klines/s. When we obtain an image with 512 (axial) × 1024 (lateral) pixels, the acquisition speed is approximately 19.5 fps. The speed of the MEMS rotational motor was set to 1,172 revolutions per minute (RPM) to be matched to an imaging speed.

3. Results

3.1 In-vivo endoscopic OCT image of airway

Figure 1 shows *in-vivo* unwrapped OCT images of the airway in a rabbit. The starting point of each 2-D image in Fig. 1(a) is slightly shifted because it was difficult to precisely synchronize the rotational speed of the motor with the acquisition speed in our OCT system. Therefore, we had to correct for starting point shift using the motor wire in the OCT images as a reference landmark. We detected the edge and the width of the motor wire using an intensity profile in

#136728 - $15.00 USD Received 18 Oct 2010; revised 21 Dec 2010; accepted 30 Dec 2010; published 5 Jan 2011

lateral direction. After detection, we laterally shifted and arranged images so that the wire was in the same location as shown in Fig. 1(b).

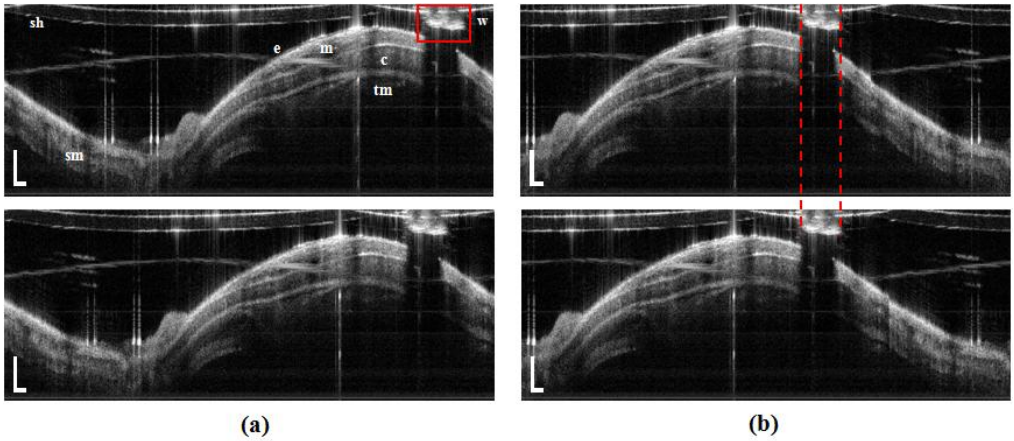

Fig. 1. *In-vivo* unwrapped OCT image of the airway in a rabbit. Distance between the upper image and lower image is longitudinally 10 intervals (200 μm). (a) images demonstrate the shift of scanning start points between two images and (b) images show correction of image movement. Scale bar is physically 500 μm (axial) and 10 deg (lateral); e- epithelium, m- mucosa, sm- submucosa, c- cartilage, tm- muscularis, sh- sheath (tube), and w- motor wire.

We used processing algorithms to construct the 3-D volume image and to measure the airway thickness [25]. First, we used the previously reported algorithms for reconstruction of 3-D volume image, which include removal of motion artifacts due to a cardiac cycle, breathing cycle, and slight whipping movement of the probe [25]. The initial longitudinal reconstruction was performed based on the unwrapped 3-D data set. The sheath and motor wire images of the probe were removed, and then the upper edge of the moving surface (blue line in Fig. 2(b)) was detected by using specified brightness in an OCT image as a threshold value. The corrected smooth surface (red line) was found by a fourth-order polynomial fit. Next, each column of the image was shifted with the difference between moving surface point and polynomial fit point. Finally, we applied a Wiener filter with 5 × 5 matrix and a median filter with 3 × 3 matrix to eliminate any white noise and speckle noise. Figure 2 shows the longitudinally reconstructed images with (Fig. 2(a)) and without (Fig. 2(c)) the realignment algorithm. Figure 2(d) shows the longitudinal airway image with flattening of the surface to measure the thickness of the mucosa and submucosa.

#136728 - $15.00 USD Received 18 Oct 2010; revised 21 Dec 2010; accepted 30 Dec 2010; published 5 Jan 2011

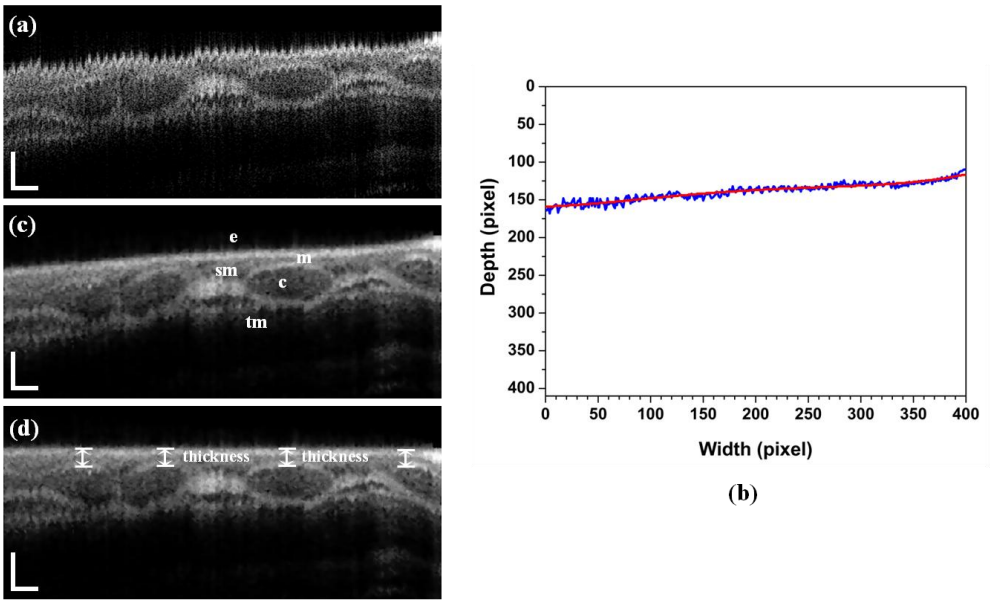

Fig. 2. *In-vivo* longitudinal OCT image of the airway in a rabbit. This longitudinal images were reconstructed with 400 B-scan slices corresponding to the physical length of 8.0 mm. (a) without motion artifacts correction, (b) surface detection (blue) and result (red) after a fourth-order polynomial fit, (c) with motion artifacts correction, and (c) with flattening of the surface to measure the thickness of mucosa in normal direction from the surface; e- epithelium, m- mucosa, c- cartilage, sm- submucosa, and tm- muscularis are clearly seen. Scale bar is physically 250 μm (axial) and 500 μm (lateral).

Figure 3 shows a representative *in-vivo* image of a normal rabbit airway with the corresponding histology. A circumferential OCT image of the airway in Fig. 3(a) was rewrapped after applying image processing algorithms. The layered structure of the airway composed of epithelium (e), mucosa (m), cartilage (c), muscularis (tm), blood vessels (BV), and peribronchial tissue (PBT) are clearly seen in Fig. 3(a). As shown in Fig. 3(b) and 3(c), the OCT image was matched well with microscopic photos of histology. Figure 3(d) shows a photo of the airway taken by a bronchoscope. Figure 4 shows a 3-D volume image and 2-D images at different viewing points. The OCT probe was placed through the endotracheal tube and extended approximately 8.0 mm beyond the end of the tube. While acquiring a 3-D data set during approximately 20 s, the OCT probe was pull and an 8-mm-long section of the airway with interval of 20 μm was scanned. Therefore, one volumetric image is constructed with 512 × 1024 × 400 voxels. The 3-D volume image of Fig. 4(a) reconstructed by commercial software, Amira (Mercury Computer System, USA) obviously shows obvious morphological features of the rabbit airway. Media 1 is a movie made with slices from inner area to outer area of the airway. Figure 4(c) and 4(d) demonstrate longitudinal images, which are arbitrarily cut at 68.5° (red) and 109.6° (blue) to the vertical direction with counterclockwise (CCW) rotation as shown in Fig. 4(b), respectively. Media 2 is also a movie constructed with cut longitudinal images from 0° to 180° with respect to the vertical axis with CCW rotation.

#136728 - $15.00 USD Received 18 Oct 2010; revised 21 Dec 2010; accepted 30 Dec 2010; published 5 Jan 2011

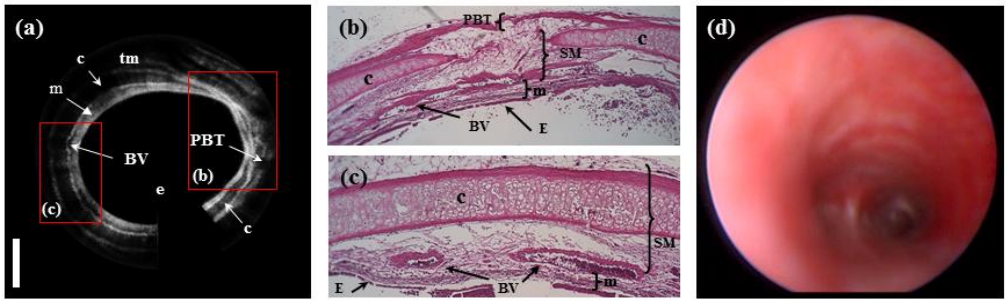

Fig. 3. (a) *In-vivo* OCT image of a normal airway in a rabbit, (b) and (c) histology, and (d) a photo of the airway taken by a bronchoscope; e- epithelium, m- mucosa, c- cartilage, BV- blood vessel, PBT- peribronchial tissue, and tm- muscularis.

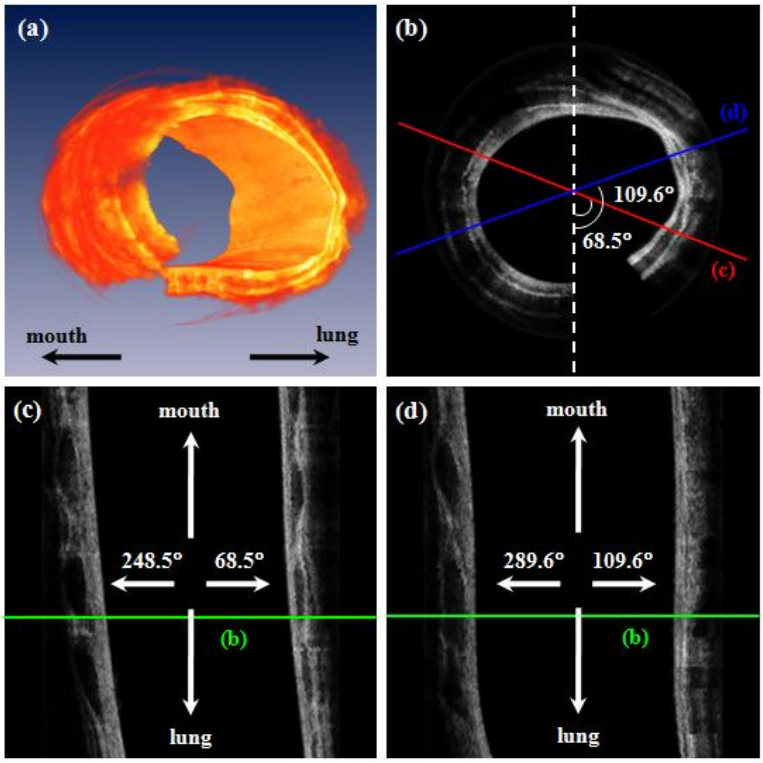

Fig. 4. *In-vivo* OCT images of normal airway in a rabbit. (a) 3-D reconstructed image based on 400 B-scan slices. (b) a circumferential 2-D image (Media 1) at one position corresponding with green lines in Fig. 4(c), and 4(d). (c) and (d) are longitudinal images, which are arbitrarily cut at 68.5° (red) and 109.6° (blue) to the vertical direction with counterclockwise (CCW) as shown in Fig. 4(b), respectively (Media 2). Media 1 is made with moved slices from inner area to outer area. Media 2 is also a movie constructed with cut longitudinal images from 0° to 180° with respect to the vertical axis with CCW rotation.

3.2 Quantification and statistical analysis of thickness change of mucosa area

The OCT probe was carefully marked for position within the endotracheal tube, then withdrawn during smoke inhalation in order to assure that smoke exposure mixed evenly and was not blocked by the presence of the OCT probe. When the OCT probe was again inserted into airway after smoke inhalation, it was positioned to the same marking point as prior to withdrawal. Thus, the location of the probe remained the same within the airways, unless any inadvertent movement of the endotracheal tube itself within the trachea had occurred. In order

#136728 - $15.00 USD Received 18 Oct 2010; revised 21 Dec 2010; accepted 30 Dec 2010; published 5 Jan 2011

to confirm that the position had not changed, the shape of airway in OCT images as shown in Fig. 1 was examined to be sure that it had not changed. However, this shape was sometimes shifted laterally. The shifted volumetric image was laterally reshifted to find same location before and after smoke inhalation. Since a reasonably long three-dimensional volumetric image of the trachea was obtained, the vast majority of the region examined would overlap, even if some small shifting of position had occurred. Furthermore measurements were made at multiple cartilaginous rings and averaged in order to overcome any variability that may have been introduced by probe movement. In our previous studies, although the surface of the longitudinal airway image has a curve or a slope as shown in Fig. 2(c), the airway thickness was measured directly [23,24]. However, the measured thickness is affected by the change of the airway surface. Therefore, we flattened and shifted the surface from Fig. 2(c) to measure accurately the airway thickness in the normal direction from the surface. Airway thickness was measured as the distance between the epithelial surface and the upper layer of cartilage rings as shown in Fig. 2(d). Airway thickness measurements were taken at 3 to 5 cartilage ring sites per longitudinal slice and 5 longitudinal slices for 3-D volumetric analyses. Measurements of the airway thickness were obtained at baseline and at each specified time period following inhalation injury. The airway thickness was averaged, and the thickness change ratio from baseline was calculated at each time point.

Differences among the cyanide infusion group (Group 1), cyanide control group (Group 2), and control group (Group 3) were determined by one-way analysis of variance (ANOVA) and two-sample *t*-test. Additionally, we performed paired-sample *t*-test to find differences between each time point. A two-tailed *p*-value less than 0.05 was considered statistically significant. All statistical analysis was performed using MATLAB (MathWorks, Inc., Natick, MA) and OriginPro (OriginLab Corporation, Northampton, MA).

In this study, 12 rabbits in total were exposed to inhaled room temperature smoke. 8 animals were exposed after post 10–30 min of cyanide injection, and 4 animals were inhaled after post 10 min of Saline injection (Table 1). Carboxy-hemoglobin levels were obtained immediately post-exposure. The ranges of carboxy-hemoglobin levels of Group 1 and Group 2 were 28.99 ± 3.52% and 36.33 ± 2.83%, respectively. There was no significant difference in the carboy-hemoglobin levels in Group 1 versus Group 2 ($p = 0.102$).

Table 1. Number of rabbits and measurement time table for cyanide poisoning and smoke inhalation study

	Group 1	Group 2	Group 3
	Cyanide injection and smoke inhalation	Saline injection and smoke inhalation	Control (only Saline injection)
Number of rabbits	8	4	4
Time table	baseline (before smoke exposure), post- 5, 15, 30, 60, 90, 120, 180, 240, 300, and 360 min (after smoke exposure)		

Figure 5 shows results of the analysis of thickness change in the airway. We found that the ratios of thickness change of Group 1 and Group 2 were increased according to expectation. Dramatic increases of thickness in the airway were seen from baseline to 30-min post-exposure in Group 1 and Group 2. At 30-min post-exposure, the mucosa thickness in Group 1 and Group 2 were increased to 42.28 ± 11.24% ($p < 0.001$) and 29.78 ± 4.10% ($p < 0.003$) compared to baseline, respectively. Airway thickness of both groups peaked at 360-min post-exposure with increases of 48.68 ± 9.25% (Group 1, $p < 0.001$) and 45.39 ± 10.14% (Group 2, $p < 0.01$). Statistically significant increases in thickness from baseline were seen at all-time points ($p < 0.01$) except for the 5 minute post exposure in Group 2; an increase of 20.36 ± 9.68% ($p = 0.078$). When we compared thickness change at one post-exposure time with it at

#136728 - $15.00 USD Received 18 Oct 2010; revised 21 Dec 2010; accepted 30 Dec 2010; published 5 Jan 2011

the others post-exposure time in Group 1, we found significant increases at 5-min and 15-min post-exposure compared to the other time points ($p < 0.03$). However, the thickness change at 5-min post-exposure has no significance compared to the change at 15-min post-exposure ($p = 0.058$). In previous studies, we demonstrated that OCT was able to detect significant thickness changes in the airway following smoke-inhalation injury (Group 2) *in vivo* [23,24].

Finally, we performed one-way ANOVA analysis to find differences among the three groups. We found significant increases of the thickness change in the airway among three groups at 30-min to 360-min post-exposure ($F > 4.0$, $p < 0.05$). However, no significant differences between Group 1 and Group 2 were seen. Significances analyzed by two-sample *t*-test among three groups are briefly summarized in Table 2.

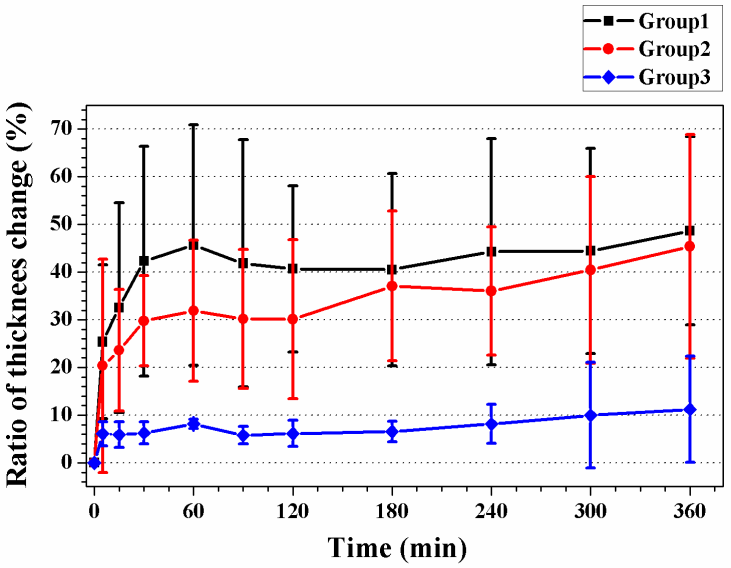

Fig. 5. Ratio of thickness change in the airway from baseline following smoke exposure or controls over time. Statistically significant from baseline were seen in Group 1 and Group 2 at all-time points ($p < 0.01$) except for 5 min post-exposure in Group 2 ($p = 0.078$). There are no significant changes from baseline in Group 3. Significant increases of the thickness change in the airway among three groups were seen at 30-min to 360-min post-exposure ($F > 4.0$, $p < 0.05$).

Table 2. *p*-values of two-sample *t*-test among three groups at 30-min to 360-min post-exposure. A *p*-value less than 0.05 was considered statistically significant

Group \ Time		30	60	90	120	180	240	300	360
Group 1	vs. Group 2	0.349	0.344	0.429	0.341	0.770	0.540	0.763	0.803
	vs. Group 3	0.015	0.016	0.022	0.003	0.008	0.014	0.014	0.006
Group 2	vs. Group 3	0.003	0.019	0.016	0.029	0.008	0.007	0.035	0.039

4. Discussion

This study demonstrates that rapid acquisition endoscopic OCT based on a swept source laser system and MEMS rotational motor, with a translational motorized stage for 3-D volumetric measurements, was able to detect significant *in-vivo* airway changes following smoke exposure. Quantitative detection of changes in thickness of mucosal region in the airway, between epithelium and cartilage were sensitively detected and followed temporally after

#136728 - $15.00 USD Received 18 Oct 2010; revised 21 Dec 2010; accepted 30 Dec 2010; published 5 Jan 2011

exposure to inhaled smoke and cyanide. Changes were evident using this technology within a few minutes following initial smoke exposure; much earlier than has been reported to be evident using standard methods [23,24,29]. The ability to detect injury following smoke inhalation or other toxic exposures is needed for an approved diagnostics, prognostics (triage and intubation decisions), and will be important in developing and accurately assessing potential therapies.

We have previously shown that OCT is capable of detecting mucosal changes and following their progression after smoke inhalation injury and half mustard injury *in vivo* in animal models [23,24,29]. However, these previous reports utilized a time domain system with limited (two-dimensional) longitudinal images due to the slow acquisition capabilities of the time domain system. Two-dimensional imaging allows only highly selected portions of the airway to be imaged, leading to potential measurement variability and selection bias. Obviously, it is necessary to find same location within the airways for measurements of the airway thickness change. When only 2-D longitudinal image without a rotational scanning is obtained, it is generally difficult or impossible to reliably maintain exact position of the prior images. With 3-D acquisition, this problem is readily solved by reconstruction in any direction. Furthermore, thickness of the submucosal region with the two-dimensional longitudinal acquisition approach is susceptible to measurement error resulting from the incident angle of the probe versus airway wall as shown in Fig. 4 and Media 2. To overcome these limitations, three-dimensional imaging with faster acquisition and the ability to reconstruct in any direction were developed for this study.

To demonstrate the capabilities for this system to detect smoke inhalation injury and followed temporally changes, we investigated three groups of animals; controls (no smoke injury), compared to animals exposed to smoke, and animals exposed to smoke and cyanide. Many smoke inhalation injury patients have concurrent cyanide exposure due to the presence of cyanide in the products of combustion. Thus, the model systems selected are relevant to human exposures, and should serve as the basis for future investigations into the effectiveness of therapeutic interventions.

Images were readily obtained in the animals using this system. Previously described algorithms were employed to eliminate cardiogenic motion artifact [25]. High quality and contrast reconstructed longitudinal images obtained from the transverse image stacks readily allowed measurement of wall airway thickness, using cartilage surfaces as the objective end-point.

In this study, we found that the thickness change of the airway was increased due to smoke inhalation in both groups of animals exposed to smoke, without significant difference in airway change from the addition of cyanide. The airway thickness changes occurred very early, within 30 minutes, and appeared to peak and level off over the period from 1 to 6 hours. The pathophysiologic events occurring during early smoke inhalation injury have been described in previous studies [2,30]. This is a cooled smoke injury animal model in which thermal effects have been eliminated. The acute injury responses are secondary to chemical/particulate injury and the immunologic responses that have been initiated. Our previous studies have shown that these early changes appear to be due to hyperemia and edema, and are clearly evident with three dimensional OCT imaging. Changes in edema and hyperemia are diminished or lost during histologic preparation, demonstrating potential value of noninvasive in vivo technologies such as optical coherence tomography to more clearly reflect events that cannot be seen with postmortem excised histologic preparations.

In this study, we did not see differences in the extent of airway changes following smoke inhalation exposure and animals receiving concurrent cyanide administration compared to smoke inhalation exposure alone. Such findings are expected, given the known initiating events in cold smoke airway injury. However, this is an important question to investigate, since many smoke inhalation injury victims are also exposed to cyanide, and studies have suggested that the cyanide blood levels correlate closely with mortality rates. One caveat to

#136728 - $15.00 USD Received 18 Oct 2010; revised 21 Dec 2010; accepted 30 Dec 2010; published 5 Jan 2011

this study is that the cyanide was administered intravenously. It is possible that inhaled cyanide concurrent with inhaled smoke could produce different results. Future studies will be needed to further assess the role of local airway effects of cyanide in smoke inhalation injury.

This study illustrates the feasibility of three-dimensional airway OCT imaging based on rapid scanning swept source laser for inhalation injury assessment. This is the first report of a series of smoke inhalation exposures followed temporally using three-dimensional airway OCT with longitudinal image reconstruction.

5. Conclusion

In this study, we obtained 3-D volumetric images of the airway in a rabbit after cyanide poisoning and smoke inhalations by means of endoscopic FD-OCT. The 3-D volumetric image approach enabled reconstruction to maintain the same position in the airway and accurate *in-vivo* quantitative thickness change determination in airways of smoke exposed rabbits. Early changes were seen in airway thickness following smoke exposures that persist throughout 6 hours of follow-up. This study demonstrates the feasibility of *in-vivo* rapid acquisition 3-D OCT that should facilitate improved clinical determination of extent of injury, prognosis, and need for intervention following smoke inhalation. Quantification of acute and longer term thickness changes of mucosa area in the airway by using *in-vivo* 3-D endoscopic OCT may provide a more sensitive tool for investigation of the effectiveness of various therapeutic interventions in smoke inhalation and other airway injuries.

Acknowledgements

The investigators would like to thank Tanya Burney for her input, advice, and guidance in the development of this study and this manuscript. This research was supported by the research grants from the National Institute of Health (R01 CA-124967-02, EB-10090, EB-00293, RR-01192), NIH CounterAct U54-NS063718-01, Air Force (FA9550-08-1-0384) and a Department of Defense SBIR award to OCT Medical, Inc. (W81XWH-09-C-0023). This work was also supported by the National Research Foundation of Korea Grant funded by the Korean Government (NRF-2009-352-D00349).

#136728 - $15.00 USD Received 18 Oct 2010; revised 21 Dec 2010; accepted 30 Dec 2010; published 5 Jan 2011